JGR Atmospheres

RESEARCH ARTICLE
10.1029/2021JD036197

Estimation of Charge Transfer During Long Continuing Currents in Natural Downward Flashes Using Single-Station E-Field Measurements

Hannes Kohlmann[1,2], Wolfgang Schulz[1], and Farhad Rachidi[2]

[1]OVE-ALDIS, Vienna, Austria, [2]EMC Laboratory, EPFL, Lausanne, Switzerland

Key Points:

- Single-station E-field measurements are used to estimate the charge transfer in 140 long continuing currents in natural downward lightning
- The estimation error, when the monopole charge model is used for transferred charge inference, is analyzed in depth
- A charge distribution model is introduced and used in a Monte Carlo simulation for the statistical evaluation of the estimation errors

Supporting Information:

Supporting Information may be found in the online version of this article.

Correspondence to:

H. Kohlmann,
h.kohlmann@ove.at

Citation:

Kohlmann, H., Schulz, W., & Rachidi, F. (2022). Estimation of charge transfer during long continuing currents in natural downward flashes using single-station E-field measurements. *Journal of Geophysical Research: Atmospheres*, *127*, e2021JD036197. https://doi.org/10.1029/2021JD036197

Received 11 NOV 2021
Accepted 8 MAR 2022

Author Contributions:

Conceptualization: Hannes Kohlmann, Wolfgang Schulz
Data curation: Hannes Kohlmann
Formal analysis: Hannes Kohlmann
Methodology: Hannes Kohlmann, Wolfgang Schulz, Farhad Rachidi
Resources: Hannes Kohlmann, Wolfgang Schulz
Software: Hannes Kohlmann
Validation: Hannes Kohlmann
Visualization: Hannes Kohlmann

Abstract The amount of charge transferred to ground during long continuing currents in natural downward flashes can be obtained either through direct current measurements or using remote electromagnetic fields, if direct measurements are not feasible. In this study, measurements of a single-station E-field antenna were used to estimate charge transfer during continuing currents. With time-synchronized high-speed video recordings serving as ground-truth data for continuing current occurrence, we estimate transferred charge during long continuing currents in 140 natural downward flashes from electric field changes, assuming a simple monopole charge model. We present average parameters for the duration, transferred charge, amplitude, and the average amplitude on five segments along the channel. Further, we perform a simulation to investigate the estimation performance of the monopole charge model, when the cloud charge is spatially extended. Using an extended charge distribution model, we generate single-station remote field waveforms and infer the charge with the monopole model. Comparison of the known and inferred charge yields estimation errors depending on the leader orientation, its spatial extension, and the observation distance. A Monte Carlo approach is carried out to statistically evaluate parameter deviations. This novel estimation error analysis sheds light on the limitations of the applied simple techniques for charge transfer estimation of long continuing currents using single-station electric field measurements.

1. Introduction

Transferred charge is an important lightning parameter in lightning protection. Continuing currents (CCs) that last from several tens to several hundreds of milliseconds give rise to thermal effects due to the high transferred charge which is much more severe compared to lightning discharges without CCs. The possible damage ranges from ignition of (forest) fires (Fuquay et al., 1967), to power line damage (Nakahori et al., 1982), to destroyed windmill blades, up to holes in metal skins of aircraft. This impacts the question of proper safety measures in many fields, where exposure to lightning discharges is relevant. Therefore, a variety of studies have already been conducted, with the goal to quantify important parameters such as the duration of CCs and their transferred charge, as well as their statistical occurrence.

In order to infer estimates of certain physical quantities of CCs, like transferred charge, charge moments, or currents and current moments, electromagnetic quantities have to be measured, either directly or remotely, and underlying physical models have to be proposed. This section is aimed at giving a comprehensive overview of lightning research literature on the evolution of various estimation methods, ranging from simple methods and instrumentation utilized in the 1950s, to more elaborated methods that were developed more recently with the goal of improving accuracy, but which require complex instrumentation setups.

A very simple, yet often used model to infer the transferred charge from the change in a remote electric field (E-field) recording dates back to the beginnings of the twentieth century. Wilson (1916) used a quasi-electrostatic relation derived from Coulomb's law to estimate charge transfers during a lightning discharge from the measured vertical electric field (E) at ground:

$$\mathrm{E} = \frac{1}{2\pi\varepsilon_0} \cdot \frac{QH}{(D^2 + H^2)^{3/2}} \tag{1}$$

where Q is the charge, H the vertical height of the charge above ground, and D the horizontal distance to the observation point (see also Uman, 1987, where Equation 1 is discussed in detail). Equation 1 was further investigated

Writing – original draft: Hannes Kohlmann, Wolfgang Schulz
Writing – review & editing: Wolfgang Schulz, Farhad Rachidi

in a broad study of E-field measurements by Pierce (1955), and Malan and Schonland (1951a, 1951b) examined processes in the interval between return strokes and charge distributions in the cloud using E-field waveforms. First important works employing multiple remote E-field antennas recording events simultaneously to estimate charge transfers, while still assuming the point charge model, can be found in Jacobson and Krider (1976), Krehbiel et al. (1979), or Brook et al. (1982). They assume a point charge model and apply the Marquardt algorithm described in Jacobson and Krider (1976). Hager et al. (2007) and Sonnenfeld and Hager (2013) extended the charge configuration model by considering a dipole and Lu et al. (2011) a time-dependent multidipole (TDMD) model to estimate charge transfers and charge distribution during intracloud lightning, using balloon-borne E-field measurements and lightning mapping array (LMA) observations. Building up on the previous methods, LMA and LEFA (Langmuir electric field array, see Sonnenfeld et al., 2009; Zhang, 2010), the leader development in the cloud during CCs was investigated (see Lapierre, 2015; Lapierre et al., 2014, 2017). Mazur and Ruhnke (2003) estimated striking distances and leader potential of first return strokes based on multistation E-field recordings assuming a line charge model.

Magnetic field (H-field) measurements have become an important means in the transient luminous events (TLEs) community to investigate the correlation of current and charge moments with the occurrence of sprites, elves, jets, and other phenomena in the upper atmosphere (refer to Füllekrug et al., 2006; Pasko, 2010). Early work treating measurements of H-fields during long CCs with fluxgate magnetometers was done by D. P. Williams and Brook (1963). To infer current and charge moments (charge transfer) from very low (VLF) or extremely low frequency (ELF) magnetic fields in a bandwidth of about 300 Hz to 22 kHz, Cummer and Inan (1997) used a model to describe the quasi-transverse-electromagnetic (QTEM) mode of atmospheric discharges (sferics) propagating along the Earth–ionosphere waveguide (see also Cummer, 2000). Received magnetic fields at very large distances (∼1,800 km) were used to estimate transferred charges between 25 and 325 C, where high charge transfer values were found to correlate with the generation of sprites. A similar model that relates remote H-fields to current moments of intense CCs was provided in Bell et al. (1998), and transferred charges ranging from 10 to 112 C during short CCs of ∼1 ms were inferred. Based on this technique, impulse charge moment changes (iCMCs) using a network of two ELF H-field antennas were evaluated for 3 years and it was estimated that 35,000 sprites occur per year over the U.S. Using the same magnetic sensor simultaneously with a shunt, the charge transfer and other characteristics of a triggered lightning event containing CC were measured in Lu et al. (2018) and Y. Fan et al. (2019). Important work was published by Ross et al. (2008) who extended Equation 1 to incorporate ionospheric interaction with the quasi-static electric field by considering ionospheric image charges. They measured quasi-static electric and magnetic fields resulting from CCs simultaneously and used the extended models to infer the estimated transferred charge and the charge moments. They presented a graph showing minimum detectable CC by E-field and H-field sensors over observation distance and showed waveforms of three cases side-by-side. For further literature related to charge transfers and charge moment changes of (TLE-producing) lightning and CCs, the reader is referred to Boldi et al. (2018), Cummer (2003), Cummer et al. (1998), Cummer and Füllekrug (2001), Cummer and Lyons (2004), Hu et al. (2002, 2007), Inan et al. (2010), Lu et al. (2009, 2012), and Ross et al. (2008).

A detailed quantitative analysis of CCs and estimation of their transferred charge, based on remote E-field measurements, was done in Brook et al. (1962). They used the monopole charge model (see Equation 1) and estimated D and H by photographs and the focal length of the lens. They reported an average duration of negative long CC (>40 ms) of 150 ms and the current magnitudes in the range from 38 to 130 A with an average of about 80 A. The transferred charges during long CCs ranged from 3.4 to 29.2 C with an average of 12 C. Kitagawa et al. (1962) reported long CC durations between 40 and 500 ms, with a mean of 180 ms. Although no charges of CCs were inferred, E-field records were used in Rakov and Uman (1990) for a broad statistical analysis of long CC occurrence as a function of various parameters (strokes per flash, stroke order, and interstroke interval duration).

By using magnetic field measurements, D. P. Williams and Brook (1963) analyzed 14 CCs with an average of 184 A of magnitude, lowering a negative charge of −31 C to ground. The average duration of the CCs was 174 ms.

Krehbiel et al. (1979) found negative CC magnitudes to be in the range of 50–580 A with a peak current occurring at the initial stage and decreasing with time at a rate of about 3–6 A/ms. Brook et al. (1982) reported CC magnitude in the range of 10 kA and transferred charge of about 300 C in Hokuriku winter storms. Based on a single-station E-field measurement, Shindo and Uman (1989) evaluated a geometric mean (GM) duration of negative long CCs of 115 ms with average amplitudes in the range from 30 to 200 A. The transferred charge

by those events was between about 3 C and a maximum of almost 40 C. Ferraz (2009) estimated values of CC following cloud-to-ground (CG) discharges, obtained from single-station E-field measurements and reported current magnitudes in the range from 30 to 1,000 A with an average of 292 A and a median of 198 A and transferred charge ranging from 1 to 370 C.

For positive CG discharges, Matsumoto et al. (1996) reported the case of a CC with an amplitude of 10 kA and 35 ms duration, that followed a natural +CG hitting a powerline. A similar result was obtained by Schumann and Saba (2012) by single-station remote E-field measurements, where they estimated currents ranging from 100 A up to 11.4 kA. Further Schumann and Saba (2012) reported for +CG transferred charges of 18–3,070 C, which is significantly higher than the charge transferred by CCs following −CG discharges.

Schumann et al. (2016) presented results, where they estimated the transferred charge from natural negative and positive downward lightning in the USA, in Austria, and in Brazil. In the USA, the average current magnitude of negative CC was 49.6 A with an average transferred charge of 10.2 C and average duration of 189.4 ms. For Austria and Brazil, the values were 68.9 A, 10.3 C, and 142.2 ms and 140.5 A, 21.2 C, and 180.1 ms, respectively. For the positive flashes in the USA/Austria/Brazil, the following results were found: 223.3 A, 67.4 C, and 285.6 ms/291.8 A, 95.5 C, and 119 ms/865.9 A, 251.2 C, and 257 ms. Tasman (2019) compared these results with the ones obtained in South Africa with a mean duration/charge of 190.7 ms/18.3 C for negative long CCs, highlighting the higher inferred charges in the southern hemisphere.

The aim of this paper is twofold: (a) to present the results and statistics of transferred charge estimations of 140 long CCs using data from a campaign that was conducted in Austria in the years 2015, 2017, and 2018 and (b) to evaluate the suitability of the monopole charge model to infer the CC transferred charge from single-station field measurements. The novelty of the presented work lies in the qualitative and quantitative analysis of the presented results, which takes into account that the evaluated data were obtained from single-station E-field measurements and that the simplicity of the considered monopole charge model will naturally lead to uncertainties in the resulting estimated charge.

The paper is organized as follows: Section 2.1 describes the measurement results and the data set of the campaign; the processing of the obtained raw data is also described in this section. Section 2.2 proceeds by introducing the method that is used to compute the transferred charge during a CC and the current waveform from the E-field data under the assumption of a monopole charge model. Since the application of a monopole charge model unavoidably introduces uncertainties through distance and height estimations of the charge center, it is useful to determine these errors quantitatively in the form of a sensitivity analysis, which is done in Section 2.3. In Section 3, the evaluated results are presented for the whole data set consisting of 17 positive and 123 negative long CCs. These results comprise (a) the average estimated charge (arithmetic and GM), (b) the cumulative probability plots of the mean CC amplitudes, and CC duration respectively, (c) a table of evaluated parameters of the used data set (minimum and maximum values of duration, current, charge, and observation distances), and (d) a segment-wise trend of the CC waveforms, where all current waveforms are normalized by their duration. In order to investigate the degree of the error that is inherent to the monopole charge model, the discussion in Section 4.1 introduces a model of a spatially extended charge distribution in the cloud, which is assumed to feed CCs in contrast to a monopole charge. This model is used to generate (simulate) remote E-field waveforms corresponding to varying spatial charge extent and distance to the observation point, respectively. On the basis of these simulated E-field waveforms with defined transferred charge, the error, respectively the accuracy, of the estimated charge when using the monopole charge model is evaluated statistically with the Monte Carlo method in Section 4.2. In this connection, the statistical performance of different parameters, like the arithmetic mean (AM), the GM, and the median of the charge of the whole data set, is investigated. Section 5 summarizes the important concepts and findings of this study.

2. Data and Methodology

2.1. Measurement and Data Set

The presence and duration of CCs in a lightning flash can be determined by inspection of high-speed video observations when available. In Diendorfer et al. (2003), it was shown that the brightness of the channel correlates strongly with the amplitude of the CC. There is no luminosity when the current in the channel is zero. Hence, for each case, the end time of the CC was determined from the video frames, where the luminosity of the channel

had completely faded. To use the same methodology as in comparable studies (e.g., Schumann et al., 2016), the starting point to compute the transferred charge in long CC was set to 5 ms after the occurrence of the radiation field peak. According to Krehbiel et al. (1979), it is a common observation that it takes up to several milliseconds for the electric field of a return stroke to settle (even though the return stroke process itself has a duration in the order of 100 μs). In Shindo and Uman (1989), it is stated that field changes within the first few milliseconds "could well be due to in-cloud processes, or to cloud-ground processes different from CC." Thus, 5 ms after the radiation field peak is considered to be a reasonable starting point for the computation of transferred charge related to long CC processes.

To record the E-field, a flat-plate antenna connected to an amplifier with an analog integrator was employed. The decay time constant of the integrator was $\tau = 0.47$ ms (E-fast). The corresponding lower cutoff frequency of $f = 340$ Hz (or an angular frequency of about 2,100 rad/s) can be found through the relation $1/\tau = \omega = 2\pi f$. The digitizer sampling frequency was 5 MHz, which, however, was limited by an upper cutoff frequency of approximately 1 MHz of the operational amplifier that was used in the analog integrator circuit. The slow E-fields were obtained in a separate step by using a decay time constant compensation method (Rubinstein et al., 2012 or Mazur & Ruhnke, 2003). The reader is encouraged to refer to Kohlmann et al. (2017), where (a) examples of the data that were obtained with the same measurement system as employed for the present campaign are shown, and (b) the performance of the decay time constant compensation method is presented.

The recordings were mostly obtained in open plains under similar conditions. However, in the process of the data curation, an empirical calibration test was performed by evaluating the ratio between return stroke peak currents inferred by the Austrian lightning location system ALDIS and the corresponding radiation field peaks in the recorded E-field. This way, days (or sites) exhibiting coarse deviations from the expected ideal calibration could be sorted out.

In most cases, a decay of the compensated E-field was observed after the termination of the CC. In theory, we would expect to see a plateau in the E-field, but intracloud processes will cause further changes in the E-field. Yet, there was a decay even in those cases, where obviously all long CC processes had ended (i.e., the luminosity on the video recording had faded). The amplifier, behaving like a differentiator at low frequencies, was equipped with an offset compensation circuit in its second stage. The E-field change caused by CC is interpreted like an offset and the compensated field therefore decays exponentially with a time constant of 6 s. The correction of this artificial decay resulted in an increase of 5% for the absolute value of transferred charge estimations. An additional phenomenon resulting in a noticeable decay after a CC process and influencing the charge estimation is the electric field recovery. This effect is described for example in Krehbiel et al. (1979), Nakano (1975), and Jacobson and Krider (1976). Depending on the distance of observation and the intensity of the lightning activity, the electric field recovery can cause either exponential or linear decay with relaxation time constants in the range of about 2 up to 30 s or more.

The influence of the ionosphere on the electric fields was treated in Ross et al. (2008). It was shown that the consideration of additional image charges (extended form of Equation 1), which satisfy the boundary conditions of the ionosphere, lead to E-fields that decrease faster than $1/r^3$ over distance. The formula given in Ross et al. (2008) was evaluated and found to reduce the E-field at a distance of 30 km by no more than 7.5%, when the ionospheric height is 59 km. The impact becomes smaller with increasing ionospheric height. Since this additional deviation is small compared to other deviations (discussed in Section 2.3), and the major part of the CCs were closer than 30 km, the influence of the ionosphere was neglected in this study.

For reducing the measurement noise (which is amplified by Equation 2, see next Section 2.2), we employed a moving average filter of 10 samples for close-distance fields (lower than about 10 km) with a good signal-to-noise ratio, and 100 samples for more distant cases.

The distance D, which is one of the two input parameters which have to be estimated prior to estimating the transferred charge using Equation 1 (see Section 1), was extracted from the known location of the strike point corresponding to the CC event, located by the Austrian lightning location system (ALDIS). In doing so, the channel transferring the charge to ground is assumed to be perfectly vertical, which introduces a distance error to be discussed in Section 2.3.

The other parameter of Equation 1 is the height H of the charge center. It can be estimated by balloon or radio soundings in regions where the main charge separation is usually assumed to prevail (see Krehbiel et al., 1979). Indeed, in Schumann et al. (2016), the height H of the negative charge center in the cloud was determined by radio soundings. The estimated values for H were obtained considering the −10°C temperature level for each day of measurement using the platform provided by the University of Wyoming, Department of Atmospheric Science (http://weather.uwyo.edu/upperair/sounding.html). For all years, Vienna radio soundings (station number 11035) were used for the respective days to estimate the height H of the charge center. The positive charge center was assumed to be 3 km higher than the estimated negative charge region at the −10° temperature level (see e.g., Lu et al., 2009, where high altitude charge regions as source of CCs following +CG strokes were assumed). Schumann et al. (2016) also made a sensitivity analysis, where the effect of a deviation of the values for the height H and the distance D of the charge center from the true values on the calculated charge Q is shown. Similar considerations can for example be found in Shindo and Uman (1989) or Uman (1987).

In this study, a total of 140 long CCs (CCs exceeding a duration of 40 ms from the beginning of the return stroke) recorded in the years 2015, 2017, and 2018 were analyzed. The data set is composed of 123 long CCs following negative cloud-to-ground strokes (−CG) and 17 following positive cloud-to-ground strokes (+CG). Due to the high sensitivity of the charge estimation to distance (due to a nonvertical channel and/or distributed charge instead of a monopole charge) and charge height deviations at close distances D to the strike point (see sensitivity analysis in Section 2.3), only lightning discharges at distances larger than 5 km were used for the evaluation. The closest discharge was at 5.1 km and the most distant was at 41.7 km. Also, we excluded field records from the evaluation that were clearly impacted by low-frequency noise, for example, caused by raindrops resulting in unwanted peaks and distortions in the field waveform or by concurrent discharges of other cells, and field waveforms which were implausible for CCs. If the resulting E-fields after the time constant compensation did not yield clearly identifiable and clean CC ramps, the CC case was removed from the set. Examples of such typical (clean) E-field waveforms related to a CC that was obtained by compensating the instrumentation decay time of the amplifier circuit can be found in Kohlmann et al. (2017) Further, Supporting Information S1 showing two cases of CCs is provided as supplemental material for this paper.

In this paper, the term "magnitude" is used when the absolute value (e.g., $|I_{cc}|$) of a parameter is of interest rather than the "amplitude," which is a signed value.

2.2. CC Charge Transfer Calculation

The transferred charge during the CC was determined by means of the compensated waveforms. To determine the transferred charge during a discharge process, we used E-field changes in conjunction with the simple monopole charge model from Equation 1. Rearranging Equation 1 gives the relation of the charge Q and vertical E-field at a remote observation point. This model (applied e.g., in Kurihara et al., 2017; Mazur & Ruhnke, 2003; Schumann et al., 2016; Shindo & Uman, 1989; Uman, 1987) assumes a monopole charge at height H above a straight vertical lightning channel at a horizontal distance D from the electric field observation point. If the change of the electric field between the times $(n-1)\cdot\Delta t$ and $n\cdot\Delta t$ is $\Delta E_n = E(n\cdot\Delta t) - E((n-1)\cdot\Delta t)$, then the related transferred charge ΔQ_n can be calculated using Equation 1. The resulting current at time $n\cdot\Delta t$ is then determined by

$$I_n = \frac{\Delta Q_n}{\Delta t} \tag{2}$$

where the sampling duration in Equation 2 was set to $\Delta t = 0.5$ ms. For the analysis of the time dependence of the CCs obtained from the compensated E-fast records using Equation 2, the CC duration was divided into five equal segments (from 5 ms after the return stroke till fully faded luminosity), for each case individually. The underlying assumption is that the shape of the waveform does not depend on the total duration. For each of those five segments, the mean I_{cc} (CC amplitude) was determined. The analysis and results of those processed I_{cc} waveforms are described in Section 3.

2.3. Monopole Charge, Sensitivity, and Error Analysis

This simple estimation method using a "charge centroid" or "monopole" (Mazur & Ruhnke, 2003; Schumann et al., 2016; Shindo & Uman, 1989; Uman, 1987) as a source for the CC is prone to considerable estimation errors,

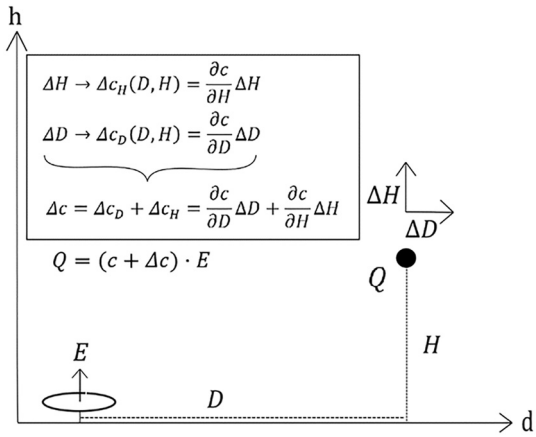

Figure 1. Total differential as estimation error, partial differentials as sensitivity of deviations in height (ΔH) and distance (ΔD).

if estimated distance and height deviate from the true monopole charge location (D, H). This is shown in Figure 1, for distance and height deviations, ΔD and ΔH. A sensitivity analysis of charge estimation errors depending on ΔD and ΔH is presented in this section. This analysis is crucial to understand the errors involved in charge estimations using single-station measurements and applying the monopole charge model (see also Shindo & Uman, 1989).

The charge Q estimated from the E-field can be written as $Q = (c + \Delta c) \cdot E$, where c is the conversion factor between E and Q (see Equation 1):

$$c(D,H) = \frac{Q}{E} = 2\pi\varepsilon_0 \frac{\left(H^2 + D^2\right)^{3/2}}{H} \tag{3}$$

Δc is a deviation (error) that is caused by distance and height estimation errors ΔD and ΔH, respectively. The total deviation Δc in the conversion factor depends on two components, Δc_D and Δc_H. It can be written as a total differential with respect to the distance and height difference ΔD and ΔH:

$$\Delta c = \Delta c_D + \Delta c_H = \frac{\partial c}{\partial D}\Delta D + \frac{\partial c}{\partial H}\Delta H \tag{4}$$

The partial derivatives of Equation 3 in Equation 4 can be found as

$$\begin{aligned} \frac{\partial c}{\partial D} &= 6\pi\varepsilon_0 \cdot \frac{D}{H}\left(D^2 + H^2\right)^{1/2} \\ \frac{\partial c}{\partial H} &= 2\pi\varepsilon_0 \cdot \left[\left(D^2 + H^2\right)^{1/2} - \frac{\left(D^2 + H^2\right)^{3/2}}{H^2}\right], \end{aligned} \tag{5}$$

representing the sensitivity of c with respect to D while H remains constant and the sensitivity of c with respect to H while D remains constant. Multiplied with ΔD and ΔH one gets a linear approximation of the error in each direction for the amount (ΔD, ΔH) of deviation. Therefore, when calculating the charge from E-fields, the total error of charge $\Delta Q_\varepsilon = \Delta c \cdot$E with Δc from Equation 4 represents the approximate total deviation of the estimated charge for sufficiently small ΔD and ΔH. Figure 2 shows the error $\varepsilon_H = \Delta c_H(D,H)|_{\Delta H = 1\,\mathrm{km}}/c(D,H)$ and $\varepsilon_D = \Delta c_D(D,H)|_{\Delta D = 1\,\mathrm{km}}/c(D,H)$ in % of the conversion factor c relative to the true factor at a given distance D and height for deviation units of $\Delta H = 1$ km (ε_H, Figure 2, top graph) and $\Delta D = 1$ km (ε_D, Figure 2, center graph). That error has to be scaled with respect to the desired deviation (e.g., a 3 km deviation results in 3 times the depicted error in the graph). The bottom graph of Figure 2 depicts the (absolute) error ratio, indicating how sensitive the height error ε_H is in relation to ε_D. It can be seen that for observation distances between 5 km and roughly 20 km (which is the dominant observation range in the field campaigns of this study), the error due to height deviation ΔH has less impact on the charge estimation than ΔD. Distance estimation errors, resulting from CC sources that are not located above the striking point (e.g., leader extension up to several kilometers within the cloud), are expected to be larger than height estimation errors, which are bound to a comparably narrow vertical range.

To give an example, we assume a true charge location is at $D = 20$ km and $H = 5$ km. Using Figure 2, center graph, for a distance deviation of $\Delta D = +3$ km (i.e., a distance overestimation of 3·1 km), the error ε_D is 3 times +14%, yielding an estimation error of +42%. An additional overestimation of height, for example, $\Delta H = +500$ m (half of 1 km), adds $\varepsilon_H = 0.5 \cdot (-17\%) = -8.5\%$ at $D = 23$ km. The total charge estimation error becomes approximately $\varepsilon_Q = 42\% - 8.5\% = +33.5\%$. Using Equation 3 directly with the erroneous distance and height estimation values ($D = 23$ km and $H = 5.5$ km) results in a higher charge overestimation of +37% due to cumulating higher estimation errors. The linear approximation is not appropriate for particularly large distance and height estimation errors. For negative distance or height errors (i.e., underestimation), the sign of the errors in Figure 2 has to be inverted.

The error sensitivity shown in Figure 2 does not consider the ionospheric impact on the E-fields, as mentioned in Section 2.1 (see also Ross et al., 2008). This effect becomes more important with increasing distance but is considered to have a negligible effect for distances lower than about 30 km.

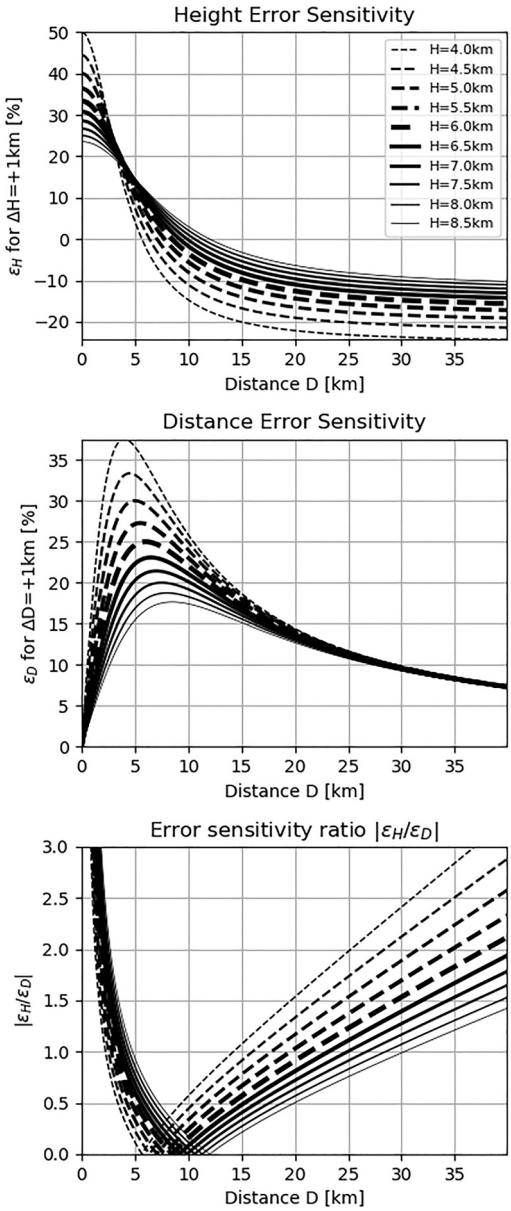

Figure 2. Approximation of the error sensitivity of c in Equation 3 in percent for a deviation of the true height by $\Delta H = 1$ km (top) and distance D by $\Delta D = 1$ km (center). The error sensitivity ratio indicates the impact (absolute value) of a height error relative to the distance error at a given (true) distance and height (bottom).

Distance errors from an equivalent monopole charge result from the location error of lightning location systems (which is in the range of 100 m), nonvertical CG discharge channels, and errors due to spatially distributed charge regions, the location errors of the LLS being negligible compared to the latter. Further, height estimation errors from radio soundings are smaller compared to distance estimation errors. Figure 2 shows that the distance error of the assumed charge position is the dominant error. The estimation error for distributed charge regions instead of a monopole model is discussed in Section 4.1.

3. Results and Analysis

In the following, the main results for CCs in –CGs and +CGs are summarized and compared to results from other studies. The CC durations are based on the luminosity of the channel in the high-speed video recordings (beginning at the time frame that contains the return stroke until the complete fading of the channel), whereas the current magnitudes and charges were calculated from the compensated remote E-fields, beginning at 5 ms after the return stroke (as already mentioned in Section 2).

For CCs following a –CG, the AM of the transferred charge, which was determined by applying Equation 1, was −24.5 C (GM −8.1 C) and the maximum observed charge was −506 C. The minimum transferred charge was −0.2 C, which occurred in a subsequent RS with long CC. Together with a mean amplitude of −126 A (median −64 A), these values are in good agreement with values in the literature (see Section 1). Further, they are in very good agreement with the results of the Austrian campaign obtained by Schumann et al. (2016) for the years 2008–2012. This was expected, since the measurement system, the region and therefore the climatic conditions, and the methodology were the same. The mean CC duration in Schumann et al. (2016) was 154 ms. On the other hand, it was 166 ms (median 140 ms) in this study. The largest observed mean CC amplitude over its duration observed in this analysis was −1,615 A, while in Schumann et al. (2016) the maximum observed mean amplitude was −793 A. The longest duration of a negative CC in our campaign was 533 ms which is in the same order as the 575 ms reported by Schumann et al. (2016).

Cumulative probability plots of the magnitude and duration for negative CGs are depicted in Figures 3 and 4, respectively. The plots of CC magnitude and CC duration are close to a straight line; hence, the values are approximately log-normally distributed. In Shindo and Uman (1989), the GM value of the CC duration of negative CC is 115 ms, which is slightly lower compared to a median of 140 ms determined by our analyses.

The obtained AM of the transferred charge for CCs following positive CGs was 117 C (GM 70 C) with a mean current magnitude of 539 A (median 407 A). Maximum values of 433 C and 1.8 kA were estimated. The average and median values for the duration were respectively 218 and 183 ms. Since the data set is relatively small, the statements about the results in comparison to other studies have to be taken with caution. The main results of our study are summarized in Table 1.

In order to analyze the changes of the current amplitude I_{cc} over the time of current flow, each CC was normalized with respect to its duration and divided into five equally long segments, whose mean current was determined. Then, the average current (AM) over all CC cases was evaluated for each segment. Finding different types of waveforms (as they are summarized in Campos et al. (2007), with six different CC types obtained from luminosity analyses of video recordings, or Fisher et al. (1993), with four different CC types obtained from direct

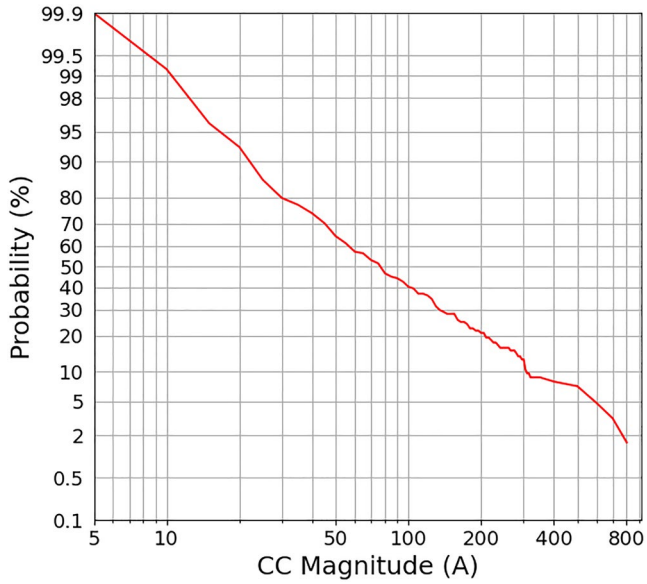

Figure 3. Cumulative probability of continuing current (CC) magnitude.

current measurements of rocket-triggered lightning), was not the goal of this approach. The main interest was to find an average trend of the CC magnitude for long CCs. In Figure 5, these values (mean/median) of the average CC of each segment are visualized by means of Box plots for CCs following a negative CG. The values start from a median of −101 A in the first segment, descending to a median of −16 A in the fifth segment.

In Figure 6, the segments for CCs following a positive CG are shown. Monotonically declining values can be observed for the mean, median, and the maximum values for both negative and positive cases, which confirms the declining characteristic of CCs found in Krehbiel et al. (1979), where a decrease rate of about 3–6 A/ms was observed for the three reported CCs following a −CG. It is worth noting, that for both cases, −CG and +CG, the mean and median values deviate due to outliers that pull up or down the AM significantly. The overall CC trend shows similar declining behavior for both, −CG and +CG. The results are summarized in Table 2.

We also analyzed the AM (GM) magnitude of the current in the first 5 ms after the return stroke of a –CG with CC, which are not part of the overall magnitude estimations. The mean magnitude of the current within the first 5 ms is on average 3.4 times (3.6 times) larger than the AM (GM of the amplitude over the full duration of the CC (see Table 1). For +CG, a factor of 3.9/2.5 (AM/GM) was found for the ratio between the mean magnitude of the first 5 ms compared to the full CC.

Another observation in this study was that in 36% of all CCs of –CGs, the E-field change had faded to zero (resulting in vanishing calculated current amplitude) before the luminosity in the video had faded to zero. In these cases, the currents were between 10% and 69%, on average 32%, shorter than in cases when luminosity was observable on video. A comparison between two E-field waveforms, where in one case the E-field reaches a plateau at an early stage, is provided in the Supporting Information S1 (see Data Availability Statement). The effect might be related to the motion of a large amount of charges which is significant enough to overdub the E-field change caused by the CC process. Another reason for faster declining fields can be the propagation direction of the leader, that successively collects and transfers charge from the cloud to ground. This motion of the charge center over time relative to the observer leads to a smaller ΔE ramp toward the end of the CC, if the active leader propagates away from the observer (see also Figure 8 in Section 4.1), such that the E-field change is no more discernable. As a third reason, a chemical afterglow process (without charge transfer) is imaginable, which can vary between individual CCs. Since an early termination of the E-field change is not observed systematically in all cases, it is not considered to be an instrumental artifact.

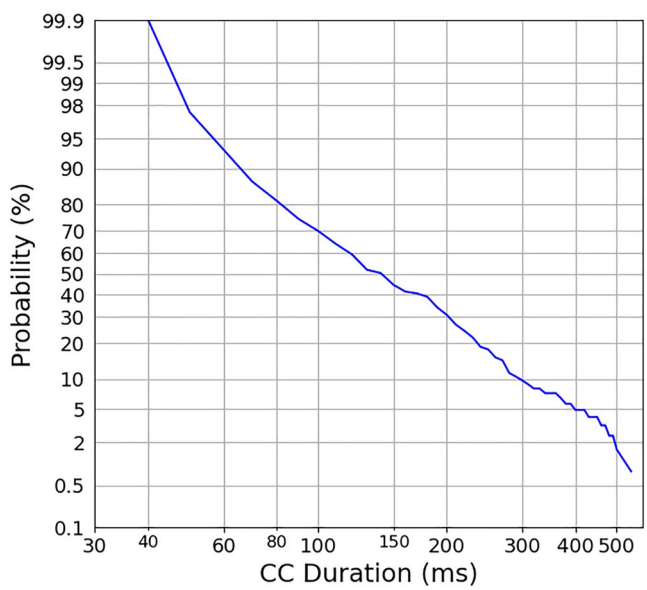

Figure 4. Cumulative probability plot of CC duration.

Assuming that the current decays linearly on average, as the evaluation in this study suggests (see Figure 5), and a spatial extent of the charge as source of CCs in the cloud, simulations of the CC waveform of remote E-fields along with charge estimation errors for individual cases and ensembles are presented in Sections 4.1 and 4.2. Additionally, the process may be further influenced by electric field recovery after a lightning discharge with large transferred charge. It causes an exponential decay into the opposite direction. As mentioned earlier, the relaxation time constant ranges from 2 up to 30 s or more (see Jacobson & Krider, 1976; Krehbiel et al., 1979; Nakano, 1975), resulting in smaller calculated currents toward the end of the CC. The shorter the time constant is, the earlier the relaxation effect becomes dominant in the change of the E-field and the estimated current will fade to zero.

In addition to the just mentioned influencing factors, any propagation of leaders within the cloud will influence the observed E-field, since those

Table 1
CC Parameters for the Analyzed Data

	−CG	+CG
Number of cases	123	17
Distance min (km)	5.1	7.5
Distance max (km)	38.2	41.7
Charge (AM/GM; C)	−24.5/−8.1	117/70
Charge min	−0.2	14
Charge max	−506	433
I_{cc} (AM/median; A)	−126/−64	+570/+524
I_{cc} min	−2.6	69
I_{cc} max	−1,615	1,800
Duration (AM/median; ms)	166/140	218/183
Duration min	37	42
Duration max	533	524

processes transport charge toward or away from the observer. They can appear in the E-field waveform not only as step-like M-components but also as more continuous charge exchange results in either subtle or more obvious changes of the remote E-field waveform, which degrade the accuracy of the charge estimation.

An attempt to find correlations of evaluated CC parameters, for example, between magnitude/charge transfer and duration, was unsuccessful as the computations did not yield meaningful regression and correlation coefficients. This is suspected to be caused by the used methodology (single-station measurements and monopole charge model), where individual charge estimations are assumed to deviate strongly from the true charge. Therefore, instead of performing a broad statistical analysis as given in Rakov and Uman (1990) or Shindo and Uman (1989), we focus on the expected methodological errors in the next section. A corresponding statistical evaluation is planned for future work.

4. Discussion on the Assumption of a Monopole Charge

Findings from LMA studies with respect to leader propagation in extended cloud charge regions from recent years, for example, Hager et al. (2007), Lu et al. (2009), Ciampa et al. (2011), and Wu et al. (2019), suggest that the source of CCs are fed by propagating leaders, thus regions of spatially extended charge in contrast to highly localized monopole charges. Especially Lapierre et al. (2014, 2017) and Lapierre (2015) have made great efforts to investigate the relationship between in-cloud leader growth and CCs. Recently, Sunjerga et al. (2020) observed "an extension over the (Säntis) tower of the horizontal part of a leader during the CC phase of a nearby CG flash." Further, recent three-dimensional numerical lightning discharge simulation models under special charging conditions suggest the existence of horizontally branched leaders of large extent in lightning discharges (see e.g., Mansell et al., 2002, 2010; Riousset et al., 2007).

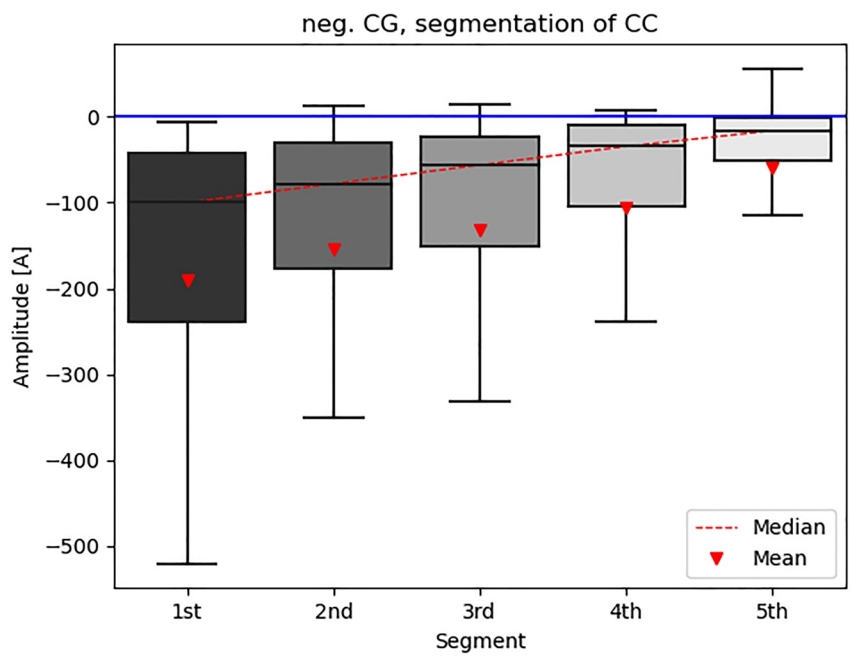

Figure 5. Box plots of the segmented continuing currents following negative cloud-to-ground (CG) discharges (123 cases).

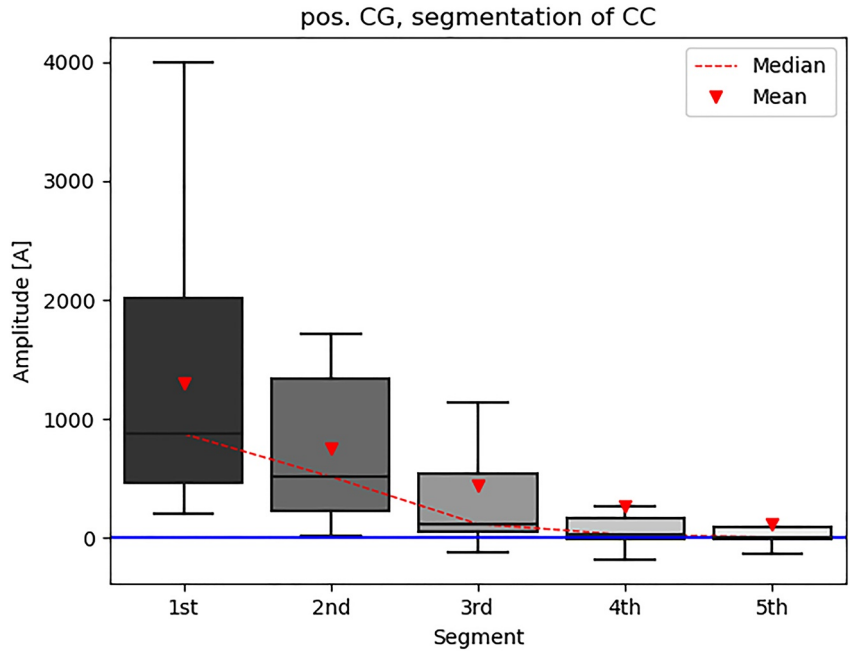

Figure 6. Box plots of the segmented continuing currents following positive CGs for the corresponding segment (18 cases).

In this section, a model that assumes spatially distributed charge as a source for CCs is introduced. The main purpose of the study is to investigate the magnitude of deviations caused by the simple static monopole model for charge transfer estimations, when in reality, the charge locations are scattered in the cloud.

The logic for the considered charge distribution model is given as follows. Even though it is a rough approximation, the results of the previous section (i.e., Figures 5 and 6) suggest that the CCs decay, on average, linearly over time. The findings from the literature given in the previous paragraphs are that (branched) cloud leaders, propagating with almost constant velocities in the order of 10^4 m/s, are the source of CCs. Thus, a spatial charge distribution model is sought for (Section 4.1), which will lead to a linearly decreasing time behavior for constant leader velocities. Later on, this model will be used to simulate E-field waveforms, which are necessary for the statistical estimation accuracy analysis in Section 4.2.

4.1. Extended Charge Distribution Model

The goal of the following extended charge distribution model, later on referred to as ECDM, is to simulate waveforms of single-station E-fields for some hypothetical spatially extended charge configurations (branches pointing into different directions away from the striking point), rather than to describe a physically supportable description of cloud charge distributions and the real mechanism of CCs.

Table 2
Segmented Analysis of CCs

	CC of –CG mean/median (A)	CC of +CG mean/median (A)
Continuing current (A)		
1st segment	−190/−101	+1,302/+876
2nd segment	−154/−78	+752/+515
3rd segment	−132/−56	+442/+117
4th segment	−105/−35	+260/+27
5th segment	−60/−16	+118/+8

As mentioned above, the cloud charge, that serves as a source for the CC, is removed by the tip of one or possibly multiple leader branches that propagate in the cloud. Thus, the charge effectively feeding the current from one branch is assumed to be a horizontal line charge with a specific line charge density function. Small portions ΔQ of available cloud charge are successively removed from their location and transferred to ground through the channel. This can be interpreted as a monopole moving with time (therefore called "dynamic monopole" in Hager et al. (2007)). Multiplying ΔQ with the factor c from Equation 3 results in ΔE, which is the corresponding change in the remote E-field. The channel is assumed to behave as a perfect conductor and behaving neutral in this CC process.

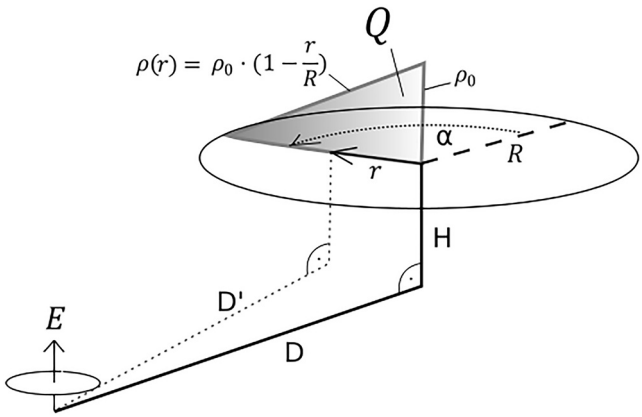

Figure 7. Linearly decaying charge distribution (gray shading) as source of CC. The circle with radius R, around the vertical channel above the strike point at distance D, indicates possible orientations of the leader in the cloud, described by the angle α.

The simple monopole charge model is obviously a very crude representation of the complex charge distribution in the cloud. In Figure 7, a more elaborate, yet simple model of a charge distribution is shown for a direction "r". This model assumes a linearly decaying charge distribution, with a line charge density (C/m) defined as

$$\rho(r) = \rho_0 \cdot \left(1 - \frac{r}{R}\right) \tag{6}$$

where ρ_0 is the line charge density at the origin of the leader. It is therefore called ECDM with linear decay (ECDM-L). It reaches zero at R and the height H is assumed to be constant over time. Instead of the physically unrealistic scenario of only one leader direction (straight extended line charge in Figure 7), this model could as well be used for several branches of different charge and extent R that are superimposed and represent different leader directions transporting charge from the cloud to ground during the CC process.

Small portions of charge $\Delta Q(r) = \rho(r) \cdot \Delta r$ are successively removed by a horizontal leader at a height H from locations indicated by r, which is at a horizontal distance D' to the observation point (see Figure 7), for small spatial steps Δr. At time t, charge is removed from the cloud at the location $r = v \cdot t$. Assuming that the leader velocity $v = dr(t)/dt$ is approximately constant and the total CC discharge duration is T_{cc}, the spatial extent R of transferred charge will be $R = v \cdot T_{cc}$. Using these simple assumptions, it can be shown that the linearly decaying line charge density (Equation 6) of the ECDM-L leads to a linearly decaying CC magnitude over time given by

$$I_{cc}(t) = \frac{dQ(t)}{dt} = \frac{\rho(vt) \cdot dr(t)}{dt} = v \cdot \rho(vt) = v \cdot \rho_0 \cdot \left(1 - \frac{v \cdot t}{R}\right) = v \cdot \rho_0 \cdot \left(1 - \frac{t}{T_{cc}}\right) \tag{7}$$

similar to the average time dependency of long CC waveforms (Figures 5 and 6) in the campaign. It shall be stressed, that ECDM-L (linearly decaying distribution) is a purely hypothetical model with the aim to reproduce this linear decay of the average current waveform evaluated in the campaign. However, the ECDM can be adjusted to represent any arbitrary spatial function for the line charge density, that could be physically more accurate.

The simulated remote E-field waveforms at the observation point for differently oriented ECDM-L distributions from $\alpha = 0°$ (away from observer) to $\alpha = 180°$ (toward the observer) are shown in Figure 8. The used distance parameters are $D = 10$ km and $H = 5$ km. The leader velocity was chosen to be$v = 2{\cdot}10^4$ m/s (see e.g., Lapierre et al., 2014). A total charge of $Q = 10$ C is transferred to ground during a total long CC discharge duration of $T_{cc} = 250$ ms, which leads to a spatial extent of $R = 5$ km. For the static monopole (black squares, in Figure 8), the curve was computed assuming transferred charge portions which correspond to a current that decays linearly with time and reaches zero at T_{cc}, and which result in a total cumulated transferred charge of $Q = 10$ C. It shall be mentioned that the choice of the time T_{cc} and the velocity v was only made to prove that ECDM-L leads to a linearly decay of the CC with time (Equation 7). However, the duration T_{cc}, the velocity v, and the absolute time t are not relevant for the statistical estimation accuracy analysis in Section 4.2. Instead, solely the amount ρ_0 and spatial position r of the transferred charge, and the spatial extent R are of importance, that is, Equation 6. The line charge density ρ_0 results from a specified spatial extent R and a specified total transferred CC charge Q (which will also serve as the reference value). R will be randomly selected and Q is assumed to be constant and equal to 10 C. The absolute spatial position of the charge is found corresponding to Figure 7, where α and D will both be randomly selected, and H is assumed to be fixed (5 km).

For comparison, the charge estimates using the (static) monopole model (by multiplying changes in the E-field with the conversion factor given in Equation 3) for the E-field waveforms corresponding to the orientation α are given in the legend of Figure 8. Thus, the charge that is distributed away from the observer results in an underestimation (e.g., −29% for $\alpha = 0°$) and when distributed toward the observer in an overestimation (e.g., +62% for $\alpha = 180°$) of the charge values. It can be interpreted as an equivalent monopole shifted horizontally away from or toward the observer, resulting in a deviation corresponding to Figure 2, center graph, in Section 2.3. One can see, that a charge distribution that is oriented toward the observer has more weight regarding the estimation error.

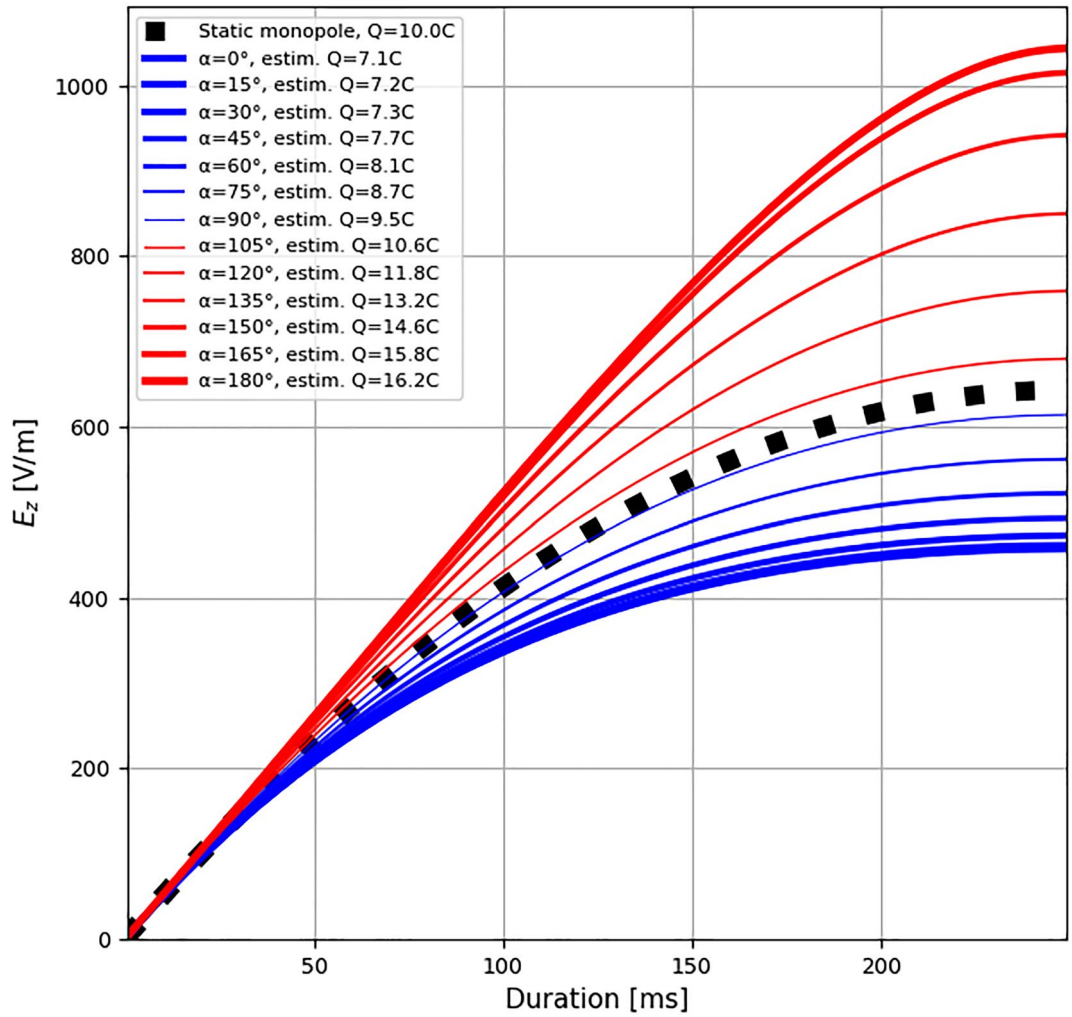

Figure 8. Remote E-field waveforms for ECDM-L of extent $R = 5$ km for a strike point distance $D = 10$ km and charge height $H = 5$ km. The legend shows estimated charge using the monopole model (Equation 1), where blue E-field waveforms lead to underestimation and red curves to overestimation of transferred charge. The ensemble AM of the charge is 10.61 C, while the GM is 10.14 C.

For the full ensemble (all depicted waveforms) of this example, the AM yields 10.61 C and the GM 10.14 C. That means that the GM of the ensemble estimates is just +1.4% higher than the true value of the assumed 10 C, whereas the AM estimates is +6.1% higher than the true value.

4.2. Statistical Estimation Accuracy Analysis

In the field campaign, we are using 123 negative CC cases. Thus, it is interesting to know how accurate the estimated results (AM, GM, median) of such a sample are, when the charge of each case is calculated from the E-field records assuming a static monopole model. Using the ECDM-L model, a Monte Carlo simulation was performed for statistically varying extended charges (uniformly distributed once with mean value $\mu_R = 5$ km and maximum extent 10 km and with $\mu_R = 10$ km and maximum extent 20 km in a second simulation) with random, uniformly distributed orientation angles (0°–360°). The charge value is fixed (10 C) for each simulation, which serves as the well-known reference value. A constant charge height ($H = 5$ km) is assumed. The distance varies in steps of 1 km in the range of $D = 0$–30 km. Using these parameters, 100 E-field waveforms (see Figure 8), resulting from the ECDM-L model (Figure 7), were generated. This is close to the sample size of negative CCs in this study. The generated E-field waveforms are then used to determine theoretical charges calculated with the static monopole model for height H and distance D, which yields charge estimates that deviate from 10 C in each

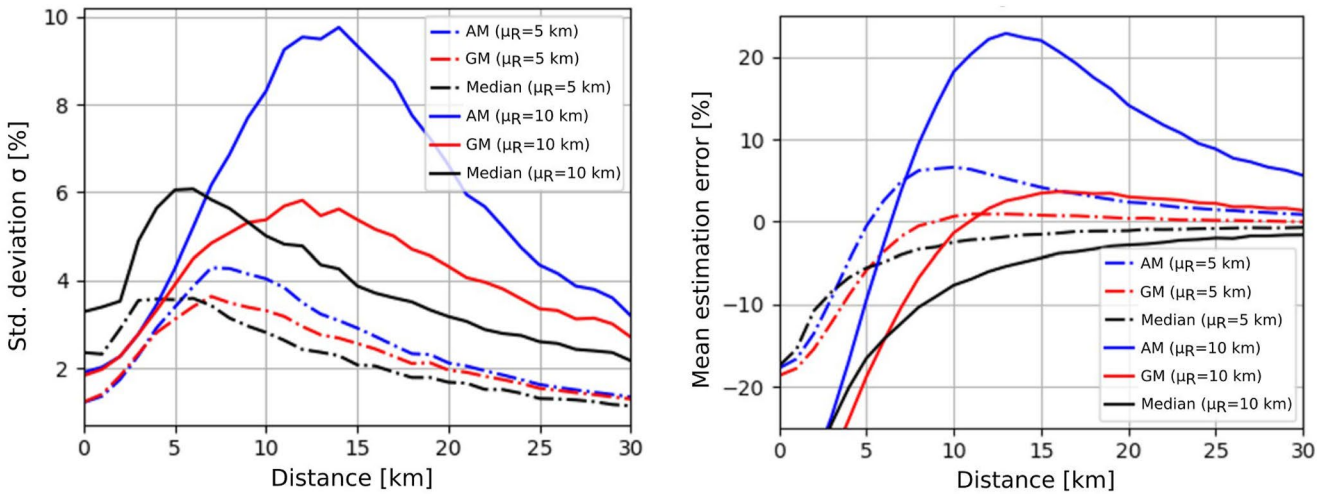

Figure 9. Charge estimation error over distance. Average estimation error (left graph) and standard deviation of the estimation error (right graph) for arithmetic mean, geometric mean, and median for ensembles of 100 charge estimations (static monopole model, Equation 3) of E-field waveforms (see Figure 8) at fixed distances D and constant height ($H = 5$ km), generated using the ECDM-L model with uniformly distributed random spatial charge extents (average extent of 5 km, dash-dotted, and 10 km, solid) and random orientation (0°–360°).

case. For every sample of E-field waveforms with random extents and orientation, the AM, GM, and median of the full ensemble have new statistically varying values. This way we determined the AM, GM, and median for 2,000 cycles (samples) and examined the resulting mean charge estimation error and its standard deviation for increasing distances D in steps of 1 km.

The behavior of the AM (blue), GM (red), and median (black) for an ensemble size of $N = 100$ charge estimations for two differently distributed charge extents (dash-dotted: $\mu_R = 5$ km, solid: $\mu_R = 10$ km) for increasing observation distance is depicted in Figure 9.

The results show that the GM is less affected by the monopole representation of horizontally extensive charge regions (e.g., $\mu_R = 10$ km) in the distance of interest, whereas the AM overestimates and the median underestimates the charge for smaller observation distances. All three estimators converge to 0% average error for observation distances greater than 30 km. It shall be noted that despite the convergence to 0% error for >30 km, a low SNR and/or height estimation errors (see Section 2.3, Figure 2, which were not considered in this simulation) will lead to weaker estimation performance. At very close distances, all estimators underestimate the true charge, and large leader extents in the cloud decrease the estimation performance further. The standard deviation (spread) of the AM estimation error is the largest, whereas the standard deviation of the GM performs better (especially for large extents, $\mu_R = 10$ km). For distances larger than 10 km, the estimation error of the median has the smallest standard deviation. Since the median is also less biased than the AM (see Figure 9, left graph), both the median and the GM perform better than the AM as an estimator of charge ensembles for distances larger than 5–10 km.

If the ensemble size N is larger, for example, $N = 200$ instead of $N = 100$, the standard deviation (Figure 9, right graph) becomes smaller for all estimators, whereas the mean estimation error (Figure 9, left graph) remains practically unchanged. The reason is that the full circle (0°–360°) in Figure 8 is filled out with CCs of differently oriented and extended leaders, which all result in an effective distance error (see Section 2.3). Thus, Figure 9 (left graph) represents the error that is due to the geometrical influence of the extended charge distribution. Further, if a different charge distribution is considered (in contrast to ECDM-L), the graphs in Figure 9 will change toward larger estimation errors if the charge distribution causes bigger effective distance errors of the equivalent static monopole charge location.

To conclude this part, it can be stated that the GM appears to be the best estimator for the CC transferred charge. It represents the ensemble average most robustly if charge from extended distributions is transported to ground by propagating leader branches using a static monopole model for charge calculation. Also, the median represents the average ensemble charge better than the AM. Although in this simulation, a constant charge was assumed, in reality, the transferred charge in CCs is expected to be log-normally distributed, where the GM and the median

values are equal. Although it does not make a big difference whether the GM or the median is used, both the GM and the median of the sample (campaign) will be more reliable estimators compared to the AM according to this evaluation.

5. Summary and Conclusion

Obtaining parameters of long CCs in natural downward flashes is important to assess the hazard related to these lightning events. While direct current measurements of long CC discharges to flat ground are not possible, data from instrumented towers which are mostly associated with upward flashes may not be fully appropriate to infer statistical data on CCs in natural downward flashes (see also E. R. Williams et al., 2012, who pointed out the "unnatural" influences of tall structures). Furthermore, spatially distributed antenna arrays for recording the electric field are difficult to install in densely populated areas. Multisensor recording in conjunction with least squares optimization algorithms (Jacobson & Krider, 1976; Krehbiel et al., 1979) allows to perform more detailed analyses with respect to the charge distribution in the cloud. However, due to their easier availability, the study was conducted using single-station measurements.

The procedure of estimating transferred charge from E-field measurements requires accurate data, especially in the field late-time response. Thus, the raw data obtained from the output of the integrator must be compensated for its limited time constant. As a further step, this allows to estimate the magnitude and the transferred charge in a return stroke or CC by applying a simple monopole charge model. Although being a simplistic method to calculate transferred charge from single-station E-field recordings, the results show good agreement with values found in literature. We used that method for analyzing 140 events in total, 123 cases of CC of –CG, for which AM values of −126 A (median −64 A) amplitude, 166 ms (median 140 ms) duration, and −24.5 C (GM −8.1 C) were obtained. For 17 cases of CC of +CG, the AM were 570 A (median 524 A), 218 ms (median 183 ms), and a charge of 117 C (GM 70 C). More results are listed in Table 1. These results give the overall impression that AM, GM, and median CC values that were obtained are in good agreement with the literature.

Although according to X. Fan et al. (2014), it is not necessarily the case that CCs have their highest magnitude at the beginning of the CC process (which is supported by findings from Campos et al. (2007), and Fisher et al. (1993)), the segmentation method in this study showed, that, on average, the CCs have a higher magnitude at the beginning, gradually descending toward the end of the process, nearly linear in the case of −CGs. The results showed a median amplitude of −101 A in the first segment and −16 A in the last segment for negative CCs. For the positive CC cases, a similar characteristic was observed although only 17 cases were considered. The first segment had a median amplitude of +876 A and the last segment +8 A.

As an alternative to the classical (static) monopole model as a source of CCs, a novel approach for modeling spatially extended charge distributions (ECDM) with linear decay of charge density with distance was introduced in Section 4.1. The hypothesis is supported by findings from LMA observations, which suggest that leader branches, propagating through the cloud, serve as a source for CCs (see Ciampa et al., 2011; Hager et al., 2007; Lapierre et al., 2014; Lu et al., 2009; Wu et al., 2019). The effect is a spatial shift of an equivalent monopole charge and results in errors which were quantified in the sensitivity analysis presented in Section 2.3. Individual CC charge estimations can exhibit very large deviations when the static monopole model is used. This error has more weight when the extended charge distribution is oriented toward the observer and is close to the observer, which was shown in an analysis for angles between 0° and 180° (Figure 8). It results in overestimation of the AM value of the ensemble. By means of a Monte Carlo simulation, it was further shown in Section 4.2, that for large spatial extents of the charge, the GM and median are the more robust parameter estimators (Figure 9) when using the monopole charge model for a data set where the spatial charge extent of individual CCs changes randomly. They yield more accurate mean charge estimation results for the data set compared to the AM by compensating for the estimation errors caused by geometrical deviations (see Section 2.3) due to extended CC sources in the cloud over the full measurement range (5–40 km). The primary purpose of introducing ECDM was to investigate the accuracy and reliability of the monopole charge model for charge transfer estimation. Future work will be laid out to validating and adapting this model based on observations (together with LMA data) and, based on the findings, to improve charge transfer estimation accuracies from single-station E-field waveforms using curve-fitting or machine learning techniques.

The significance of this study lies in the fact that only few campaigns dealing with a large data set of CCs in natural downward lightning exist in the literature. Simple but well-known analytical and numerical techniques were combined to estimate transferred charge during long CCs. Because of the technical and logistical challenge to obtain multistation synchronized E-field records, single-station observations will still remain an important means to estimate charges of CCs in natural lightning. Thus, researchers should be aware of the performance limitations and error behavior of the applied simple techniques, which is what we analyzed in depth and presented in this work.

Data Availability Statement

The repository https://doi.org/10.6084/m9.figshare.16989220 provides all continuing currents evaluated from the compensated E-fields as spread sheets (first column: time stamp in seconds, second column: current values in Ampere). In addition, graphs of the computed continuing current waveforms were uploaded. The labels in the graphs contain information on the used and evaluated parameters, for example, the assumed cloud charge height H, observation distance D, and the computed transferred charge for the given continuing current event. A Supporting Information S1 provides an example case of a continuing current, where the E-field change terminates significantly earlier than the observed luminosity in the video recordings.

Acknowledgments
Since getting useful data sets in lightning research is a challenging task, we want to thank Christian Vergeiner and Lukas Schwalt for their efforts of obtaining great E-field and high-speed video recordings during the lightning season over the years and having evaluated many parameters beforehand. Further we want to thank Jeff Lapierre for sharing his valuable experience that he gathered while dealing with continuing currents, LEFA, and LMA in the course of his PhD studies. Special thanks go to Gerhard Diendorfer whose willingness for creative scientific discussion has been of great help throughout this work.Open access funding enabled and organized by Projekt DEAL.

References

Bell, T. F., Reising, S. C., & Inan, U. S. (1998). Intense continuing currents following positive cloud-to-ground lightning associated with red sprites. *Geophysical Research Letters*, *25*(8), 1285–1288. https://doi.org/10.1029/98GL00734

Boldi, R., Williams, E. R., & Guha, A. (2018). Determination of the global-average charge moment of a lightning flash using Schumann resonances and the LIS/OTD lightning data. *Journal of Geophysical Research: Atmospheres*, *123*, 108–123. https://doi.org/10.1002/2017JD027050

Brook, M., Kitagawa, N., & Workman, E. J. (1962). Quantitative study of strokes and continuing currents in lightning discharges to ground. *Journal of Geophysical Research*, *67*(2), 649–659. https://doi.org/10.1029/JZ067i002p00649

Brook, M., Nakano, M., Krehbiel, P. R., & Takeuti, T. (1982). The electrical structure of the Hokuriku winter thunderstorms. *Journal of Geophysical Research*, *87*(C2), 1207. https://doi.org/10.1029/JC087ic02p01207

Campos, L. Z. S., Saba, M. M. F., Pinto, O. J., & Ballarotti, M. G. (2007). Waveshapes of continuing currents and properties of M-components in natural negative cloud-to-ground lightning from high-speed video observations. *Atmospheric Research*, *84*(4), 302–310. https://doi.org/10.1016/j.atmosres.2006.09.002

Ciampa, K., Beasley, W. H., & Petersen, D. A. (2011). *Comparing high-speed video and Lightning Mapping Array observations to investigate the influence of ground strikes on lightning flash characteristics*. Paper presented at American Geophysical Union, Fall Meeting, abstract id AE13A-0377. Retrieved from https://ui.adsabs.harvard.edu/abs/2012AGUFMAE13A0377C/abstract

Cummer, S. A. (2000). Modeling electromagnetic propagation in the Earth–ionosphere waveguide. *IEEE Transactions on Antennas and Propagation*, *48*(9), 2–12. https://doi.org/10.1109/8.898776

Cummer, S. A. (2003). Current moment in sprite-producing lightning. *Journal of Atmospheric and Solar-Terrestrial Physics*, *65*(5), 499–508. https://doi.org/10.1016/S1364-6826(02)00318-8

Cummer, S. A., & Füllekrug, M. (2001). Unusually intense continuing current in lightning produces delayed mesospheric breakdown. *Geophysical Research Letters*, *28*(3), 495–498. https://doi.org/10.1029/2000GL012214

Cummer, S. A., & Inan, U. S. (1997). Measurement of charge transfer in sprite-producing lightning using ELF radio atmospherics. *Geophysical Research Letters*, *24*(14), 1731–1734. https://doi.org/10.1029/97GL51791

Cummer, S. A., Inan, U. S., Bell, T. F., & Barrington-Leigh, C. P. (1998). ELF radiation produced by electrical currents in sprites. *Geophysical Research Letters*, *25*(8), 1281–1284. https://doi.org/10.1029/98GL50937

Cummer, S. A., & Lyons, W. A. (2004). Lightning charge moment changes in U.S. High Plains thunderstorms. *Geophysical Research Letters*, *31*, L05114. https://doi.org/10.1029/2003GL019043

Diendorfer, G., Viehberger, M., Mair, M., & Schulz, W. (2003). An attempt to determine currents in lightning channel branches from optical data of a high speed video system. In *International Conference on Lightning and Static Electricity (ICOLSE)* (pp. 3–6).

Fan, X., Zhang, G., Wang, Y., Li, Y., Zhang, T. T., & Wu, B. (2014). Analyzing the transmission structures of long continuing current processes from negative ground flashes on the Qinghai–Tibetan Plateau. *Journal of Geophysical Research: Atmospheres*, *119*, 1063–2050. https://doi.org/10.1002/2013JD020402

Fan, Y., Lu, G., Li, X., Zheng, T., Zhang, H., Jiang, R., et al. (2019). Measurements of magnetic pulse bursts during initial continuous current of negative rocket-triggered lightning. *Journal of Geophysical Research: Atmospheres*, *124*, 11710–11721. https://doi.org/10.1029/2019JD031237

Ferraz, E. d. C. (2009). *Measuring of continuing currents in natural negative cloud-to-ground lightning on Brazil: Development of equipment and first results (PhD thesis)*.

Fisher, R. J., Schnetzer, G. H., Thottappillil, R., Rakov, V. A., Uman, M. A., & Goldberg, J. D. (1993). Parameters of triggered-lightning flashes in Florida and Alabama. *Journal of Geophysical Research*, *98*(D12), 22887–22902. https://doi.org/10.1029/93JD02293

Füllekrug, M., Mareev, E. A., & Rycroft, M. J. (2006). *Sprites, elves and intense lightning discharges*. Retrieved from https://books.google.com/books?hl=de&lr=&id=XagIZhRZvRoC&oi=fnd&pg=PR12&dq=füllekrug+sprites+elves+and+intense&ots=YAwNXThlvG&sig=rNDZsxH9s5QzVQlY7BV7SNvPoQs

Fuquay, D. M., Baughman, R. G., Taylor, A. R., & Hawe, R. G. (1967). Characteristics of seven lightning discharges that caused forest fires. *Journal of Geophysical Research*, *72*(24), 6371–6373. https://doi.org/10.1029/JZ072i024p06371

Hager, W. W., Sonnenfeld, R. G., Aslan, B. C., Lu, G., Winn, W. P., & Boeck, W. L. (2007). Analysis of charge transport during lightning using balloon-borne electric field sensors and Lightning Mapping Array. *Journal of Geophysical Research*, *112*, D18204. https://doi.org/10.1029/2006JD008187

Hu, W., Cummer, S. A., & Lyons, W. A. (2007). Testing sprite initiation theory using lightning measurements and modeled electromagnetic fields. *Journal of Geophysical Research*, *112*, D13115. https://doi.org/10.1029/2006JD007939

Hu, W., Cummer, S. A., Lyons, W. A., & Nelson, T. E. (2002). Lightning charge moment changes for the initiation of sprites. *Geophysical Research Letters*, *29*(8), 1279. https://doi.org/10.1029/2001GL014593

Inan, U. S., Cummer, S. A., & Marshall, R. A. (2010). A survey of ELF and VLF research on lightning-ionosphere interactions and causative discharges. *Journal of Geophysical Research*, *115*, A00E36. https://doi.org/10.1029/2009JA014775

Jacobson, E. A., & Krider, E. P. (1976). Electrostatic field changes produced by Florida lightning. *Journal of Atmospheric Sciences*, *33*(January), 103–117. https://doi.org/10.1175/1520-0469(1976)033<0103:EFCPBF>2.0.CO;2

Kitagawa, N., Brook, M., & Workman, E. J. (1962). Continuing currents in cloud-to-ground lightning discharges. *Journal of Geophysical Research*, *67*(2), 637–647. https://doi.org/10.1029/JZ067i002p00637

Kohlmann, H., Schulz, W., & Pichler, H. (2017). Compensation of integrator time constants for electric field measurements. *Electric Power Systems Research*, *153*, 38–45. https://doi.org/10.1016/j.epsr.2016.07.014

Krehbiel, P. R., Brook, M., & McCrory, R. A. (1979). An analysis of the charge structure of lightning discharges to ground. *Journal of Geophysical Research*, *84*(C5), 2432–2456. https://doi.org/10.1029/JC084iC05p02432

Kurihara, S., Nakata, H., Hashimoto, Y., & Michishita, K. (2017). A verification of estimation accuracy of lightning current waveform and charge transfer from measured E-field waveform. *Electrical Engineering in Japan*, *198*(3), 77–85. https://doi.org/10.1002/eej.22928

Lapierre, J. L. (2015). *On the relationship between in-cloud lightning activity and continuing current*. New Mexico: New Mexico Institute of Mining and Technology. Retrieved from https://ui.adsabs.harvard.edu/abs/2015PhDT20L/abstract

Lapierre, J. L., Sonnenfeld, R. G., Edens, H. E., & Stock, M. (2014). On the relationship between continuing current and positive leader growth. *Journal of Geophysical Research: Atmospheres*, *119*, 12479–12488. https://doi.org/10.1002/2014JD022080

Lapierre, J. L., Sonnenfeld, R. G., Stock, M. G., Krehbiel, P. R., Edens, H. E., & Jensen, D. (2017). Expanding on the relationship between continuing current and in-cloud leader growth. *Journal of Geophysical Research: Atmospheres*, *122*, 4150–4164. https://doi.org/10.1002/2016JD026189

Lu, G., Cummer, S. A., Blakeslee, R. J., Weiss, S. A., & Beasley, W. H. (2012). Lightning morphology and impulse charge moment change of high peak current negative strokes. *Journal of Geophysical Research*, *117*, D04212. https://doi.org/10.1029/2011JD016890

Lu, G., Cummer, S. A., Li, J., Han, F., Blakeslee, R. J., & Christian, H. J. (2009). Charge transfer and in-cloud structure of large-charge-moment positive lightning strokes in a mesoscale convective system. *Geophysical Research Letters*, *36*, L15805. https://doi.org/10.1029/2009GL038880

Lu, G., Fan, Y., Zhang, H., Jiang, R., Liu, M., Qie, X., et al. (2018). Measurement of continuing charge transfer in rocket-triggered lightning with low-frequency magnetic sensor at close range. *Journal of Atmospheric and Solar-Terrestrial Physics*, *175*, 76–86. https://doi.org/10.1016/j.jastp.2018.02.010

Lu, G., Winn, W. P., & Sonnenfeld, R. G. (2011). Charge transfer during intracloud lightning from a time-dependent multidipole model. *Journal of Geophysical Research*, *116*, D03209. https://doi.org/10.1029/2010JD014495

Malan, D. J., & Schonland, B. F. J. (1951a). The distribution of electricity in thunderclouds. *Proceedings of the Royal Society of London. Series A*, *209*(1097), 158–177. https://doi.org/10.1098/rspa.1951.0195

Malan, D. J., & Schonland, B. F. J. (1951b). The electrical processes in the intervals between the strokes of a lightning discharge. *Proceedings of the Royal Society of London. Series A*, *206*(1085), 145–163. https://doi.org/10.1098/rspa.1951.0061

Mansell, E. R., MacGorman, D. R., Ziegler, C. L., & Straka, J. M. (2002). Simulated three-dimensional branched lightning in a numerical thunderstorm model. *Journal of Geophysical Research*, *107*(D9), 4075. https://doi.org/10.1029/2000JD000244

Mansell, E. R., Ziegler, C. L., & Bruning, E. C. (2010). Simulated electrification of a small thunderstorm with two-moment bulk microphysics. *Journal of the Atmospheric Sciences*, *67*(1), 171–194. https://doi.org/10.1175/2009JAS2965.1

Matsumoto, Y., Sakuma, O., Shinjo, K., Saiki, M., Wakai, T., Sakai, T., et al. (1996). Measurement of lightning surges on test transmission line equipped with arresters struck by natural and triggered lightning. *IEEE Transactions on Power Delivery*, *11*(2), 996–1002. https://doi.org/10.1109/61.489361

Mazur, V., & Ruhnke, L. H. (2003). Determining the striking distance of lightning through its relationship to leader potential. *Journal of Geophysical Research*, *108*(D14), 4409. https://doi.org/10.1029/2002JD003047

Nakahori, K., Epawa, T., & Mitani, H. (1982). Characteristics of winter lightning currents in Hokuriku district. *IEEE Transactions on Power Apparatus and Systems*, *101*(11), 4407–4412. https://doi.org/10.1109/TPAS.1982.317407

Nakano, M. (1975). Electric field recovery after lightning flash and regeneration of charge in thundercloud. *Journal of Meteorological Society of Japan*, *53*(3), 196–202.

Pasko, V. P. (2010). Recent advances in theory of transient luminous events. *Journal of Geophysical Research*, *115*, A00E35. https://doi.org/10.1029/2009JA014860

Pierce, E. T. (1955). Electrostatic field-changes due to lightning discharges. *Quarterly Journal of the Royal Meteorological Society*, *81*(348), 211–228. https://doi.org/10.1002/qj.49708134808

Rakov, V. A., & Uman, M. A. (1990). Long continuing current in negative lightning ground flashes. *Journal of Geophysical Research*, *95*(D5), 5455–5470. https://doi.org/10.1029/JD095iD05p05455

Riousset, J. A., Pasko, V. P., Krehbiel, P. R., Thomas, R. J., & Rison, W. (2007). Three-dimensional fractal modeling of intracloud lightning discharge in a New Mexico thunderstorm and comparison with lightning mapping observations. *Journal of Geophysical Research*, *112*, D15203. https://doi.org/10.1029/2006JD007621

Ross, M. A., Cummer, S. A., Nielsen, T. K., & Zhang, Y. (2008). Simultaneous remote electric and magnetic field measurements of lightning continuing currents. *Journal of Geophysical Research*, *113*, D20125. https://doi.org/10.1029/2008JD010294

Rubinstein, M., Bermúdez, J.-L., Rakov, V. A., Rachidi, F., & Hussein, A. M. (2012). Compensation of the instrumental decay in measured lightning electric field waveforms. *IEEE Transactions on Electromagnetic Compatibility*, *54*(3), 685–688. https://doi.org/10.1109/TEMC.2012.2198482

Schumann, C., & Saba, M. M. F. (2012). Continuing current intensity in positive ground flashes. In *31st International Conference on lightning Protection (ICLP)* (pp. 1–5). Vienna, Austria: IEEE. https://doi.org/10.1109/ICLP.2012.6344260

Schumann, C., Saba, M. M. F., Paiva, A. R., Kohlmann, H., Schulz, W., Diendorfer, G., et al. (2016). Charge transfer in natural negative and positive downward flashes. In *29th International Conference on Lightning Protection (ICLP)* (Vol. 4, pp. 6–11). Estoril, Portugal.

Shindo, T., & Uman, M. A. (1989). Continuing current in negative cloud-to-ground lightning. *Journal of Geophysical Research*, *94*(D4), 5189–5198. https://doi.org/10.1029/JD094iD04p05189

Sonnenfeld, R. G., Eack, K., Eastvedt, E., Edens, H. E., Hager, W. W., Hunyady, S., et al. (2009). *Development of the Langmuir electric field array (LEFA)*. Paper presented at American Geophysical Union, Fall Meeting, abstract id AE43B-0265. Retrieved from https://ui.adsabs.harvard.edu/abs/2009AGUFMAE43B0265S/abstract

Sonnenfeld, R. G., & Hager, W. W. (2013). Electric field reversal in sprite electric field signature. *Monthly Weather Review*, *141*(5), 1731–1735. https://doi.org/10.1175/MWR-D-12-00220.1

Sunjerga, A., Rubinstein, M., Pineda, N., Mostajabi, A., Azadifar, M., Romero, D., et al. (2020). LMA observations of upward lightning flashes at the Säntis Tower initiated by nearby lightning activity. *Electric Power Systems Research*, *181*(July), 106067. https://doi.org/10.1016/j.epsr.2019.106067

Tasman, J. D. (2019). *Inference of charge transfer from lightning flashes in South Africa*. Retrieved from http://wiredspace.wits.ac.za/handle/10539/29157

Uman, M. A. (1987). The lightning discharge. *International Geophysics Series*, *39*(11), 377. https://doi.org/10.1016/0004-6981(89)90280-1

Williams, D. P., & Brook, M. (1963). Magnetic measurements of thunderstorm currents: 1. Continuing currents in lightning. *Journal of Geophysical Research*, *68*(10), 3243–3247. https://doi.org/10.1029/JZ068i010p03243

Williams, E. R., Kuo, C. L., Bór, J., Stori, G., Newsome, R., Adachi, T., et al. (2012). Resolution of the sprite polarity paradox: The role of halos. *Radio Science*, *47*(2), 1–12. https://doi.org/10.1029/2011RS004794

Wilson, C. T. R. (1916). On some determinations of the sign and magnitude of electric discharges in lightning flashes. *Proceedings of the Royal Society of London. Series A, Containing Papers of a Mathematical and Physical Character*, *92*(644), 555–574. https://doi.org/10.1098/rspa.1916.0040

Wu, B., Lyu, W., Qi, Q., Ma, Y., Chen, L., Zhang, Y., et al. (2019). Synchronized two-station optical and electric field observations of multiple upward lightning flashes triggered by a 310-kA +CG flash. *Journal of Geophysical Research: Atmospheres*, *124*, 1050–1063. https://doi.org/10.1029/2018JD029378

Zhang, J. (2010). *Development and test of the Langmuir electric field array*. Retrieved from http://kestrel.nmt.edu/$~$rsonnenf/atmospheric/2009/Zhang_thesis_20100402.pdf